ACS APPLIED MATERIALS & INTERFACES

Research Article

www.acsami.org

Surface Morphology-Dependent Photoelectrochemical Properties of One-Dimensional Si Nanostructure Arrays Prepared by Chemical Etching

Shao-long Wu,[†] Long Wen,[‡] Guo-an Cheng,*,[†] Rui-ting Zheng,[†] and Xiao-ling Wu[†]

[†]Key Laboratory of Beam Technology and Material Modification of the Ministry of Education, College of Nuclear Science and Technology, Beijing Normal University, Beijing 100875, China

[‡]Key Laboratory of Material Physics, Institute of Solid State Physics, Chinese Academy of Sciences, Hefei 230031, China

Supporting Information

ABSTRACT: Maximizing the optical absorption of one-dimensional Si nanostructure arrays (1DSiNSAs) is desirable for excellent performance of 1DSiNSA-based optoelectronic devices. However, a quite large surface-to-volume ratio and enhanced surface roughness are usually produced by modulation of the morphology of the 1DSiNSAs prepared in a top-down method to improve their optical absorption. Surface recombination is mainly determined by the surface characteristics and significantly affects the photogenerated carrier collection. In this paper, we systematically investigated the photoelectrochemical characteristics of 1DSiNSAs with various morphologies prepared by the metal-assisted chemical etching of Si wafers. Our results show that the saturation photocurrent density and photoresponsivity of 1DSiNSAs first increased and then gradually decreased with an increasing etching time, while the reflection spectrum was gradually suppressed to the measurable minimum. To identify the behaviors of the photoresponsivity and optical absorption of the various 1DSiNSAs, we analyzed the morphology, structure, and minority-carrier lifetime. Additionally, device physics simulations were used to confirm the significance of surface recombination. We proposed that future directions for the design of nanostructure-based optoelectronic devices should include not only strong optical absorption but also low surface carrier recombination. High-performance devices could be obtained only by balancing the requirements for light absorption and photogenerated carrier collection.

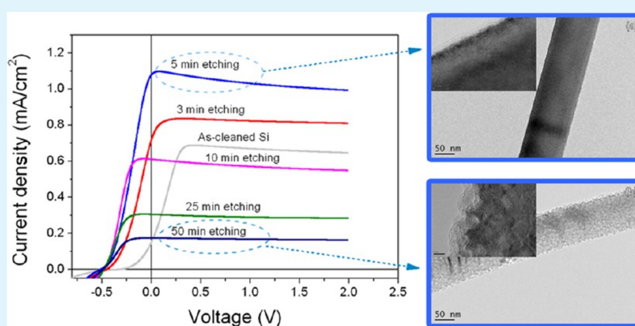

KEYWORDS: *photoelectrochemical properties, silicon nanostructures, surface recombination, optical absorption*

1. INTRODUCTION

In recent decades, one-dimensional semiconductor nanomaterials have attracted much attention because of their special morphology and unique physical and chemical properties. Among these materials, one-dimensional silicon nanostructures (1DSiNSs) are important and intriguing because of their compatibility with modern Si-based microelectronics as well as their extraordinary properties, with promising applications in photovoltaics,[1] photodetectors,[2] photoelectrolysis or photocatalysis,[3,4] sensors,[5] and thermoelectricity,[6] among others.

Various methods have been used to prepare 1DSiNSs, such as vapor−liquid−solid growth, solid−liquid−solid growth, and oxide-assisted growth. 1DSiNSs synthesized using these bottom-up methods generally have relatively smooth surfaces with fewer defects than those obtained using a top-down method via the dry (or wet) etching of bulk Si. However, the bottom-up process usually requires complicated equipment and is relatively expensive, and large-area well-aligned one-dimensional Si nanostructure arrays (1DSiNSAs) are obtained with great difficulty. Recently, a new top-down method, metal-assisted chemical etching, has been developed and widely used to synthesize the large-area well-aligned 1DSiNSAs because of its simple operation and low cost.[7−9] Many studies of the optoelectronic properties of the 1DSiNSAs prepared via this method have compared the optoelectronic performances of the 1DSiNSA and the planar Si, with varying results.[10−13] Moreover, efforts have been made to improve the optical absorption of the 1DSiNSAs by modulating their shapes and distribution and then predict an enhancement in the device performances relative to periodic cylinder nanowires,[14,15] which were demonstrated to exhibit good optical absorption.[16,17] However, few studies have provided a thorough discussion of the influences of nanostructure morphology on the optoelectronic properties, despite its decisive role in surface recombination, which is closely related to the collection efficiency of the photogenerated carrier.[18,19] Herein, we

Received: January 8, 2013
Accepted: May 13, 2013
Published: May 13, 2013

 © 2013 American Chemical Society

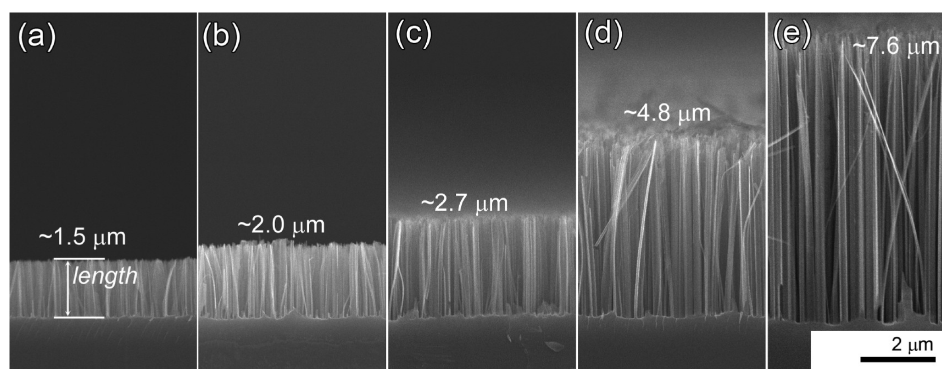

Figure 1. Typical cross-sectional SEM images of the 1DSiNSAs prepared with etching times of 3 (a), 5 (b), 10 (c), 25 (d), and 50 min (e). All the figures are shown using the same scale.

prepared 1DSiNSAs with different morphologies by the chemical etching of Si wafers. Their photoelectrochemical characteristics were systematically investigated. To identify the causes of the different photoelectrochemical responses, we analyzed the structure, optical reflectance, and minority-carrier lifetime. We also designed a physics device model to simulate and discuss the influences of surface recombination on the 1DSiNSA photoelectrochemical response.

2. EXPERIMENTAL SECTION

2.1. Preparation of 1DSiNSAs. Vertically well-aligned 1DSiNSAs were prepared by the chemical etching of Si(100) wafers with a resistivity of 2−2.7 Ω cm and a thickness of ~450 μm. As described in other reports,[19,20] the cleaned Si chips were first dipped in dilute HF for 2 min to remove the oxide layer and then immersed in a mixed aqueous solution of 0.02 M $AgNO_3$ and 4.8 M HF for the electroless deposition of Ag nanoparticles (AgNPs) for 60 s. Next, they were quickly transferred into a mixed aqueous solution of 0.2 M H_2O_2 and 4.8 M HF for chemical etching of Si for various periods of time (3−50 min). Finally, the as-etched Si was washed with deionized water and soaked in 50% HNO_3 to remove the residual AgNPs. The metal nanoparticles or ionic contamination was completely removed in the process (see Figure S1 of the Supporting Information). All the operations were conducted at room temperature.

2.2. Physical Characterization. The morphological and structural characterizations of 1DSiNSAs were performed using a field emission scanning electron microscope (FE-SEM, S-4800, Hitachi) and a high-resolution transmission electron microscope (HR-TEM, JEM-2010, JEOL). Energy-dispersive X-ray (EDX) spectra were also obtained by the FE-SEM. The optical reflectance spectra were obtained by a UV−vis spectrophotometer equipped with an integrating sphere (SPECORD 200, Analytik Jena AG). A Semilab WT-2000 microwave photoconductive decay (μ-PCD) system was used to measure the minority-carrier lifetime.

2.3. Photoelectrode Preparation and Photoelectrochemical Measurements. The photoelectrodes were prepared by sputtering an aluminum layer with an ~1 μm thickness on the backs of the 1DSiNSAs and the planar Si. Postannealing was conducted at 800 °C for 30 min in a furnace at a low pressure (~1×10^{-2} Pa) under a H_2 atmosphere. The photoelectrochemical characteristics were measured in a homemade system composed of an electrochemical workstation (CS300, Wuhan Corrtest Instrument Co. Ltd.), an electrolytic cell with a transparent quartz window, and a light irradiation system (Shenzhen LTWG Electronics Co. Ltd.). The measurements were taken in a two-electrode configuration. 1DSiNSAs and planar Si were used as the photoelectrodes, and a Pt mesh was used as a counter electrode and a reference electrode, as shown in Figure 3a. All the voltage values in this article were with respect to the Pt electrode. The irradiation source was a yellow light with a wavelength range of 590−595 nm and an irradiation intensity of approximately 41.75 W m^{-2} as measured by a commercial Si photodetector (DSi200, UV-100L, Zolix Instrument Co. Ltd.). The photoelectrodes were attached to the cell through an O-ring, and the active area was approximately 1.227 cm^2. The electrolyte solution was a mix of 40 wt % hydrogen bromide and 3 wt % liquid bromine (4:1 by volume).

2.4. Photoelectrode Response Simulations. Device physics simulations were performed using commercial electronic design automation software (Synopsys TCAD Sentaurus Device version D-2010.03) to simulate the photoelectrochemical behaviors of the 1DSiNSAs and the planar Si under steady-state operation.[18,21] Three-dimensional simulations were performed for the 1DSiNSA photo-electrodes using the photogeneration profiles calculated from finite-difference time-domain (FDTD) simulations. The film photoelectrode was simulated in a two-dimensional (2D) model using the Beer−Lambert optical excitation profile. The 1DSiNSAs were approximated as periodic cylinders on a film, as shown in Figure 6a, using the drift-diffusion carrier transport model and considering doping-dependent carrier mobility and lifetime, Auger, Shockley-Read-Hall (SRH), and surface-SRH recombination. For the 1DSiNSA simulations, a 3 nm surface layer was used to model the effects of surface traps. In all simulations, the Si−electrolyte contact (namely, the nanowire surfaces and the top surfaces of the substrate without the nanowire−substrate interfaces) was approximated as the Schottky contact with an interfacial equilibrium barrier height of 1 eV.[18] Back contact was regarded as a perfect Ohmic contact. According to the experimental parameters, the Si was uniformly phosphorus-doped at a concentration of 2.34×10^{15} cm^{-3}. The illumination source was 590 nm light with a power density of 47.15 W m^{-2}, and its incident direction was perpendicular to the film or nanowire-array surface.

3. RESULTS AND DISCUSSION

To study the effects of the 1DSiNSA morphology on its optoelectronic properties, we prepared five 1DSiNSAs by adjusting the etching time. Figure 1 shows typical cross-sectional SEM images of different samples. It can be observed that the lengths of the 1DSiNSA substantially increased from 1.5 to 7.6 μm as the etching time increased from 3 to 50 min, which can be attributed to the increased extent of Si etching according to the mechanism of the chemical etching of bulk Si.[9,22] Cross-sectional shapes of the resulting 1D Si nanostructures were nonuniform and asymmetrical, and most of the diameters were in the range of 80−300 nm (as demonstrated in our previous work[19]). Because the original morphologies of the AgNPs, which determines the diameters and density of the resulting 1D Si nanostructures,[9,19,22] on the Si wafers before chemical etching were quite similar for the different samples, the differences in the diameters of the different nanostructures prepared with different etching times were negligible.

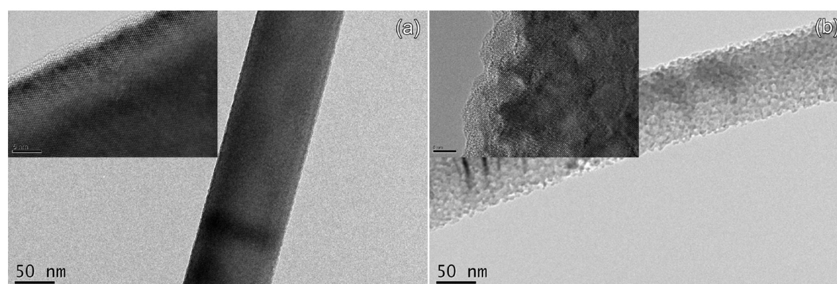

Figure 2. Typical TEM images of the single 1D silicon nanostructure from the 5 min etching (a) and 50 min etching (b) 1DSiNSAs. The insets provide the corresponding HRTEM images.

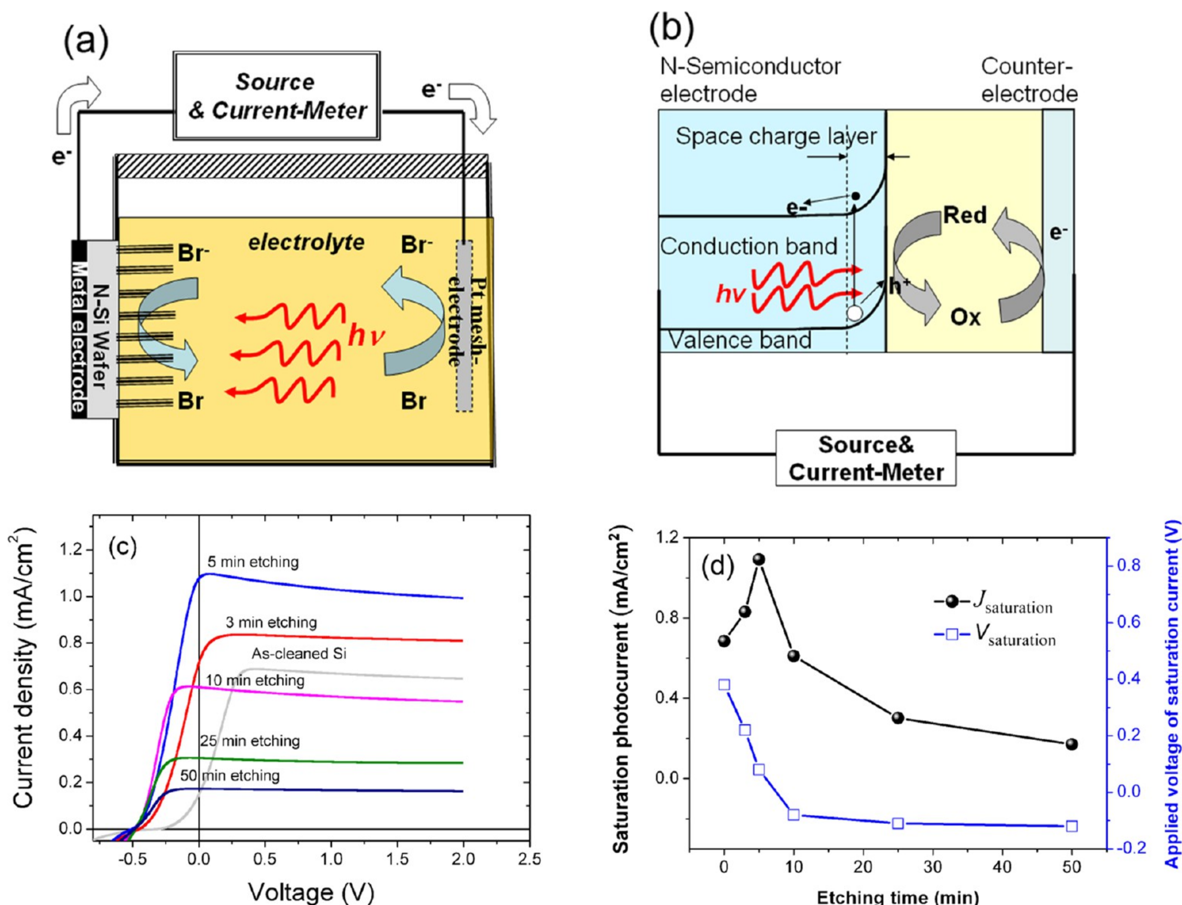

Figure 3. (a) Schematic of the measuring system of the 1DSiNSA photoelectrochemical characteristics. (b) Energy band diagram of the 1DSiNSA photoelectrodes under light irradiation without bias. (c) Photocurrent density vs voltage of the Si-based photoelectrodes prepared using different etching times. (d) Saturation photocurrent density and corresponding applied voltage as a function of etching time.

TEM analysis was used to further analyze the surface roughness and structure of the nanostructures. We found that all the orientations of the 1D Si nanostructures were along the [100] direction, which agreed with the SEM observations. The nanostructure surfaces of the different samples were slightly different: when the etching time was short (<10 min), the surfaces were nearly identical and smooth, whereas when the etching time was long (>30 min), the surfaces were rough. Figure 2 shows typical surface appearances and nanostructure structures of the 5 min etching and 50 min etching samples. The differences in the surface roughness can be ascribed to the secondary chemical etching of Si.[19] A few Ag^+ ions may deviate from the as-deposited AgNPs, depositing on the side walls of the as-etched nanostructures, and/or excess holes may diffuse from the Si under the AgNPs to the side walls of the as-etched nanostructures if the rate of hole consumption at the Si−metal interface is lower than the rate of hole injection, leading to the secondary chemical etching of the nanostructures.[23] As the etching time increases, the effect of the secondary etching accumulates, resulting in an increase in the surface roughness. Therefore, the etching time affects not only the length of the 1DSiNSs but also the surface topography.

Figure 3a shows a schematic of the photoelectrochemical response measuring system. Only a partial region of the photoelectrode was active and constantly in contact with the electrolyte. Light passed through the cell window and electrolyte and then irradiated the samples. Figure 3b shows the energy band diagram of an n-type semiconductor

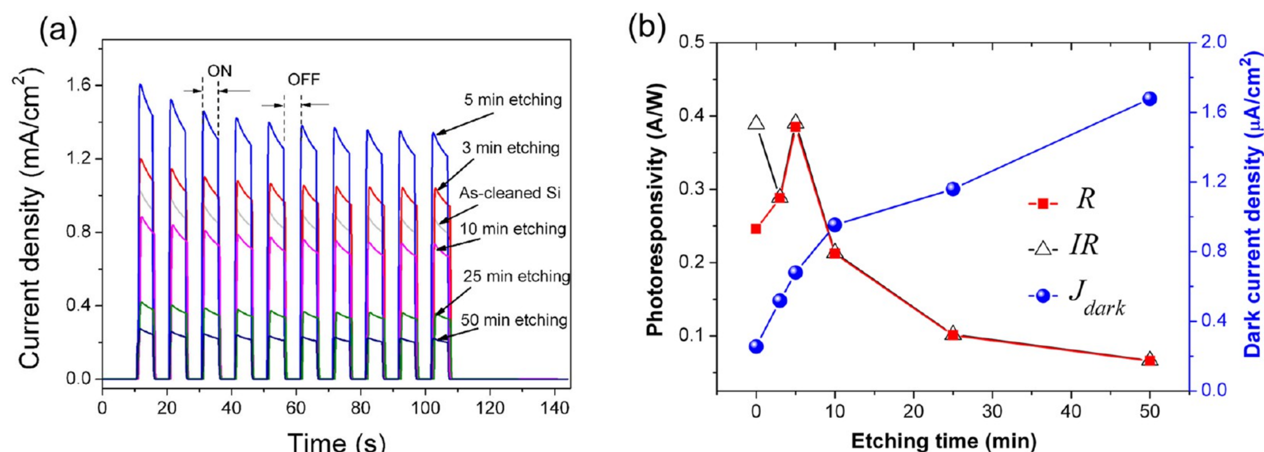

Figure 4. (a) Current density vs measuring time of the Si-based photoelectrodes prepared with different etching times under ON−OFF cycle illumination at a 1.0 V bias. (b) Overall photoresponsivity (R), internal photoresponsivity (IR), and OFF-state current density (J_{dark}) as a function of etching time.

photoelectrode under light irradiation without a bias. According to the theory of the electrochemistry of semiconductors,[24,25] when an n-type semiconductor is immersed in an electrolyte solution, the electrons will be transferred into the solution because the Fermi level of the electrode is typically higher than the redox potential of the electrolyte. There is a positive charge associated within the space charge layer, resulting in an upward bending of the energy band edges. Upon irradiation, the photogenerated carriers are dissociated by the built-in field; that is, the electrons are promoted to the conduction band and then transferred into the Si interior, whereas the holes are transferred into the solution to oxidize Br^-, leading to a measurable photocurrent.

Figure 3c shows the photocurrent density versus voltage of the Si-based photoelectrodes prepared with different etching times. All the samples exhibited photoelectrochemical responses: as the biases were applied from a negative value (−1.0 V) to a positive value (2.0 V), the corresponding photocurrent densities changed from negative values to positive values and then increased to a saturation point. The saturation photocurrent of the as-cleaned polished Si (~0.685 mA cm^{-2}) was moderately high, lower than that of the 3 min etching (~0.831 mA cm^{-2}) and 5 min etching (~1.092 mA cm^{-2}) samples but higher than that of the 10 min etching (~0.611 mA cm^{-2}), 25 min etching (~0.302 mA cm^{-2}), and 50 min etching (~0.171 mA cm^{-2}) samples. The applied voltage of the saturation photocurrent of the original polished Si was the highest (0.38 V), and that of the 50 min etching 1DSiNSAs was negative (−0.12 V), suggesting the photocurrent can reach saturation without additional bias. As shown in Figure 3d, the applied voltage of the saturation photocurrent density of the Si-based photoelectrode decreased with an increasing etching time, even without an external voltage. This difference may be attributed to their different morphologies. For the 1DSiNSA photoelectrode, the semiconductor−electrolyte interfaces are three-dimensional, which is more favorable for photogenerated carrier collection than the planar interfaces.[10] As the etching time increases, the length of the 1D nanostructures gradually increases. As a result, less light penetrates into the planar substrate, the average transport distances for carrier collection are shorter, and the junction area is larger, so the photogenerated carriers can be more easily extracted out into the surface layer for the longer etching time samples.[13]

Figure 4a shows the current density versus measuring time of the Si-based photoelectrodes prepared with different etching times under ON−OFF cycle illumination at a 1.0 V bias. The current densities showed obvious alteration between the ON and OFF states. The ON-state current density of the 5 min etching sample was the highest (~1.60 mA cm^{-2}), and that of the 50 min etching sample was the lowest (~0.27 mA cm^{-2}), which is consistent with the corresponding relationship between the saturation photocurrent densities. The overall OFF-state current densities were very small because of the rectifying effect.[25] Figure 4b shows that the OFF-state current density of the as-cleaned polished Si was the lowest (~0.255 μA cm^{-2}) and that of the 1DSiNSAs increased as the etching time increased. A slight increase in the OFF-state current densities of the Si-based photoelectrodes with an increase in the etching time can be ascribed to an increase in the junction and surface area and thus recombination centers.[13] The photoresponsivity (R) was calculated via the following equation:

$$R = \frac{J_{pc}}{P_{opt}} = \frac{J_{ph} - J_{dark}}{P_{opt}} \quad (1)$$

where J_{pc} is the photogenerated current density, J_{ph} is the ON-state current density, J_{dark} is the OFF-state current density, and P_{opt} is the illumination power density. In our experiments, the maximal R of the polished Si was 0.246 A W^{-1}, higher than that of the 10 min etching (0.212 A W^{-1}), 25 min etching (0.101 A W^{-1}), and 50 min etching (0.066 A W^{-1}) samples, but lower than that of the 3 min etching (0.288 A W^{-1}) and 5 min etching (0.385 A W^{-1}) samples, as summarized in Figure 4b. The R of the 5 min etching sample was 56.5% greater than that of the planar Si, but the R of the 50 min etching sample was 26.8% less than that of the planar Si. Note that there was a slight decay for the saturation photocurrent density and the ON-state current density with an increase in the applied voltage and the ON-state time, which may come from the surface trapping of the photogenerated carriers and an increase in the series resistance.[12,13,26]

To identify the underlying physical causes of the different saturation photocurrent densities and photoresponsivities of the Si-based photoelectrodes with different morphologies, we measured the optical reflectance and minority-carrier lifetime. Figure 5a shows the diffuse reflectance spectra of the five

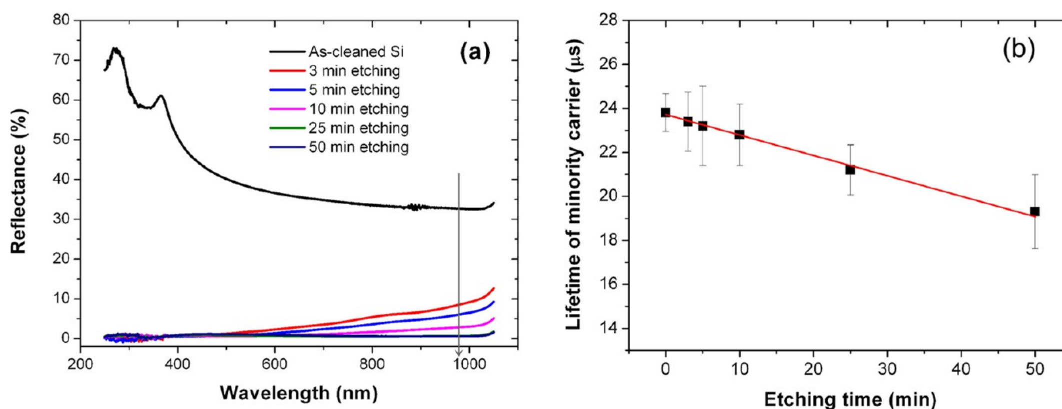

Figure 5. (a) Hemispherical optical reflectance spectra (a) and minority-carrier lifetimes (b) of the different 1DSiNSAs with various etching times and the as-cleaned Si. The direction of the arrows indicates an increase in etching time.

1DSiNSAs and the as-cleaned Si, from which the following can be noted. (1) After chemical etching, the reflectance of the as-cleaned Si was greatly suppressed in the wavelength range of 250−1050 nm. (2) As the etching time increased, the reflectance was further suppressed. (3) The reflectance of the 25 min etching sample reached the minimal measurable value, and the average reflectance below 1000 nm was <1%. (4) The reflectance spectra of the 25 min etching and 50 min etching samples nearly overlapped. The reflectance suppression arises from the low effective refractive index, and the perfect refractive index matching at the top interfaces between the air and 1DSiNSAs leads to good coupling of the incident light into the 1DSiNSAs.[16,27−29] A reduction in the 1DSiNSA reflectance with an increasing etching time is mainly due to an increase in the nanostructure length. However, when the length reaches a certain value, a further increase will not lower the optical reflectance because a negligible amount of short-wavelength light (such as visible light) can reach the nanostructure−substrate interfaces.[17] Therefore, the ultralow reflectance suggests that the 1DSiNSAs possess excellent broadband optical absorption, which is a major advantage for cost-efficient 1DSiNSA-based optoelectronic devices. For the 590−595 nm incident light, all five 1DSiNSAs exhibited very low average reflectance (<2.2%), which was much lower than that of the polished Si (∼36.8%). However, the saturation photocurrent density and photoresponsivity of the planar Si were not the lowest (but intermediate), and the disparities in the saturation photocurrent densities and photoresponsivities of the different 1DSiNSAs were relatively large. Accordingly, we deduce that the optical absorption is not the only decisive factor for the photoelectrochemical responses of the Si-based photoelectrodes in our experimental measurements.

The minority-carrier lifetime of the Si material is one of the key parameters affecting the performances of the Si-based optoelectronic devices. Figure 5b shows the minority-carrier lifetimes of the as-cleaned polished Si and the five 1DSiNSAs. The average lifetime of the original Si wafer was 23.8 μs, which decreased to 19.3 μs after the 50 min etching treatment. The linear fitting of the results indicated that the average minority-carrier lifetime decreased as the etching time increased. The measured lifetime (τ_{meas}) was a result of the combined effects of the bulk lifetime (τ_{bulk}) and the surface lifetime (τ_{surf}). For a Si film, τ_{meas} (regarded as the effective lifetime) can be expressed as[30]

$$\frac{1}{\tau_{meas}} = \frac{1}{\tau_{bulk}} + \frac{1}{\tau_{diff} + \tau_{surf}};\ \tau_{diff} = \frac{d^2}{\pi^2 D_{n,p}};\ \tau_{surf} = \frac{d}{2S} \quad (2)$$

where τ_{diff} is the diffusion time of the minority carrier from the bulk to the surface, d is the sample thickness, S is the surface recombination velocity, and D_n and D_p are the diffusion coefficients of an electron and hole, respectively. For a 1D Si nanostructure, the effective carrier lifetime (τ_{eff}) can be expressed as[31,32]

$$\frac{1}{\tau_{eff}} = \frac{1}{\tau_{bulk}} + \frac{4S}{\Phi} \quad (3)$$

where Φ is the nanostructure diameter and τ_{bulk} is the carrier lifetime of bulk Si with the same impurity concentration. The measured lifetimes of the five 1DSiNSA samples were a joint outcome of the effective lifetimes of the Si nanostructures and the planar substrate. Although we could not directly obtain the values of the surface lifetime, bulk lifetime, or effective lifetime of the Si nanostructures form these measurements of minority-carrier lifetime, we reached the following conclusions by comparisons with the different measured lifetimes of the different samples and eqs 2 and 3. (1) There was a substantial decrease in the minority-carrier lifetime of the Si nanostructures compared to that of the original planar Si. (2) The decrease in the measured lifetime was caused by a great increase in the extent of surface recombination. (3) The surface recombination velocity in the Si nanostructures prepared by chemical etching increased with an increasing etching time.

To estimate the photoresponses of the different 1DSiNSAs and the planar Si without the effect from the difference in the optical absorption, we calculated the internal photoresponsivity (IR) defined as R divided by average absorption (AA). Because the thickness of Si substrates was several hundreds of micrometers, the transmission in the range of 590−595 nm can be approximated to zero.[33] Therefore, AA can be obtained by 1 − AR (average reflectance). As calculated in this method, the IR of the planar Si was 0.3889 A W^{-1}, and the IR values of the 1DSiNSAs produced by chemical etching for 3, 5, 10, 25, and 50 min were 0.2886, 0.3902, 0.2135, 0.1017, and 0.0666 A W^{-1}, respectively (as compared in Figure 4b). One can see that only the 5 min etching sample showed a slightly larger IR via comparison to that of the planar Si, and the other 1DSiNWA samples exhibited IR values smaller than that of the planar Si. It suggests that the collection efficiency of the photogenerated

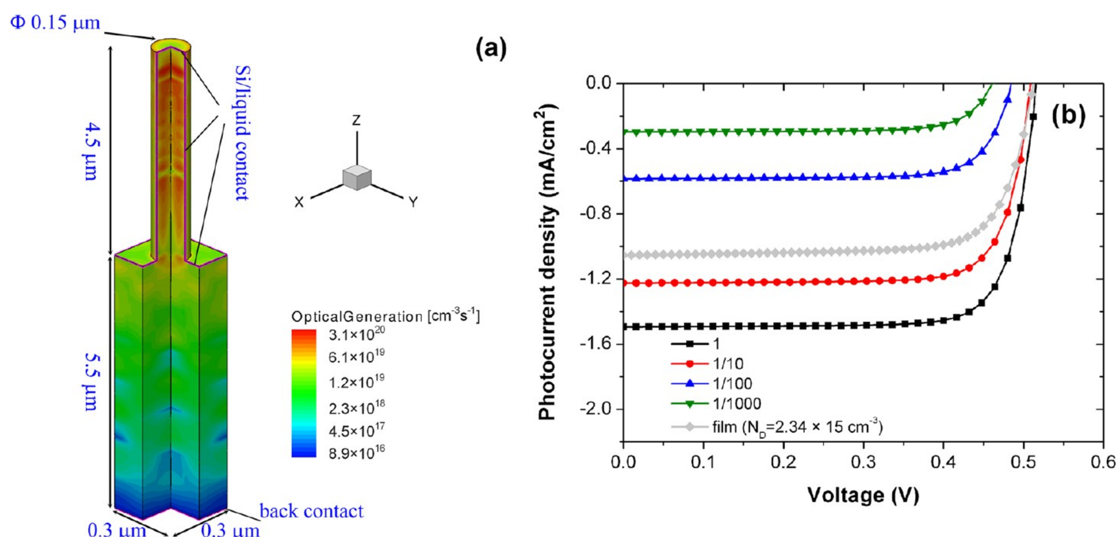

Figure 6. (a) Schematic illustration of the simulated wire array unit cell and the corresponding photogeneration profile with 590 nm light irradiation. More details of the simulated device structure and the calculated photogeneration profile are shown in Figures S2−S4 of the Supporting Information. (b) Photocurrent density vs voltage characteristics of the photoelectrodes of bare planar Si and wire arrays on Si film with various surface-layer carrier lifetimes. The full sets of optoelectronic parameters used in these simulations are listed in Table S1 of the Supporting Information.

carriers in the 1DSiNSAs is of no obvious advantage over that of the planar Si, which is ascribed to a great increase in the extent of surface recombination. However, the 1DSiNSAs prepared with short etching times showed substantially larger R values than the planar Si because of the combined effects of the much larger optical absorptivity and the comparable collection efficiency of the photogenerated carrier. The initial increase and then gradual decrease in the photoresponsivity of the 1DSiNSAs with an increasing etching time can be explained as follows. The shorter etching time 1DSiNSAs have much better optical absorption, a higher surface recombination velocity, and a larger surface-to-volume ratio than the planar Si; however, as the etching time increases, the surface recombination velocity and the surface-to-volume ratio increase dramatically, whereas the optical absorption remains nearly constant for the longer-etching samples. These results and analysis imply that surface recombination deserves special attention in nanostructure-based optoelectronic devices.

To explore the effect of surface recombination on the performances of the 1DSiNSA-based optoelectronic devices, device physics simulations were performed to simulate the photocurrent versus voltage behaviors of the photoelectrodes of 1DSiNSAs and planar Si. We employed uniform and periodic nanowires (with a diameter of 0.15 μm and a length of 4.5 μm) on a film (with a thickness of 5.5 μm) as the calculated cell (with a lattice constant of 0.3 μm) to simulate the 1DSiNSA photoelectrode, as shown in Figure 6a. The photogeneration profile shown in Figure 6a indicates that most of the incident light was absorbed by the nanowires, only some penetrated into the substrate, and little passed through the substrate. Therefore, the 5.5 μm thick film was sufficiently thick to simulate the experimental substrate, although its actual thickness was several hundreds of micrometers. In all simulations, bulk and surface recombination were modeled with a single trap level located at the energy of the intrinsic Fermi level approximately in the center of the bandgap.[18] For the nanowire simulations, the surface recombination was characterized by the surface-layer carrier lifetime, which changed in the range of 1 to 1/1000 of the doping-dependent bulk carrier lifetime. For the film simulations, the surface-layer carrier lifetime was approximated as the bulk carrier lifetime considering its small specific surface area and defect-free surface. Figure 6b shows the photocurrent density versus voltage characteristics of the photoelectrodes of a bare Si film and wire arrays on a film with various surface-layer carrier lifetimes. The following observations can be made. (1) When the surface-layer carrier lifetime was equal to the bulk lifetime, the short-circuit current density of the photoelectrode of nanowire arrays (1.494 mA cm^{-2}) was much larger than that of the film photoelectrode (1.052 mA cm^{-2}). (2) As the surface-layer carrier lifetime decreased, the short-circuit current density gradually decreased. (3) When the surface-layer carrier lifetime decreased to 1/100 of the bulk carrier lifetime, the short-circuit current density (0.585 mA cm^{-2}) was lower than that of the film photoelectrode. If the surface-layer carrier lifetime decreased further to 1/1000 of the bulk carrier lifetime, the short-circuit current density decreased substantially, reaching a value much lower (0.296 mA cm^{-2}) than that of the film photoelectrode. Note that the open-circuit voltages exhibited a relatively small variation with the change in the surface-layer carrier lifetime, which can be attributed to the variation of the short-circuit current density and the exchange current density at zero bias for solar cell device physics.[34] The simulation results demonstrate that the surface recombination has significant effects on the photogenerated carrier collection for the 1DSiNSA-based optoelectronic devices.

According to the SEM and TEM analysis, the shapes and sizes of the cross section of the 1D nanostructures prepared by metal-assisted chemical etching are asymmetrical and nonuniform, and the 1D nanostructure arrays are also disordered. The nonperiodic arrays possess better absorption than the periodic arrays, and the optical trapping among the asymmetrical 1D nanostructures is stronger than among the symmetrical 1D nanostructures.[35,36] Thus, almost all of the short-wavelength light is absorbed by the nanostructures in practice (namely, the actual level of optical absorption by the substrate is much lower than the simulation results), and the influences of the surface recombination on the carrier collection should be more profound in reality than in the simulations. Recently, some

researchers have tried to lower the level of nanostructure surface recombination to improve the performance of nanostructure-based devices by surface passivation[21,37] or surface fictionalization.[38] We believe that surface recombination can also been suppressed via the preparation of the nanostructures with smoother surfaces and fewer surface defects using a more facile method. Although the experimental and simulated results focus on the Si nanostructures, our inferences can be applied to other semiconductor nanostructures. We anticipate that high-performance semiconductor nanostructure-based optoelectronic devices can be obtained only by balancing the requirements for light absorption and photogenerated carrier collection.

4. CONCLUSIONS

We have investigated the photoelectrochemical characteristics of the 1DSiNSAs with different morphologies prepared by the chemical etching of Si for various durations. The 5 min etching 1DSiNSAs had the highest saturation photocurrent density, the 50 min etching 1DSiNSAs the lowest, and the original Si an intermediate value. The applied voltage of the saturation photocurrent density of the original Si was the highest, and that of the 1DSiNSs decreased with an increasing etching time. At a 1.0 V bias under ON−OFF cycle illumination, the maximal photoresponsivity of the 5 min etching 1DSiNSAs was 0.385 A W^{-1} and that of the samples with a >10 min etching time was smaller than that of the original Si. The OFF-state current densities of all the Si-based photoelectrodes were very low relative to the ON-state current densities and increased as the etching time increased. TEM analysis indicated that the surface roughness of the nanostructures gradually increased with an increasing etching time. The optical absorption of the 1DSiNSAs increased as the etching time increased and reached the maximal measurable value after the etching time exceeded 25 min. However, the measured minority-carrier lifetime of the 1DSiNSAs decreased gradually as the etching time increased. The device simulations demonstrated that surface recombination played a significant role in carrier collection for the nanostructure-based devices. We conclude that the performance of the semiconductor nanostructure-based optoelectronic devices is determined by the combination effects of light absorption and photogenerated carrier collection. Further improvements may be achieved using the optimal doping concentration and device structure and lowering the level of surface recombination via surface treatment or the optimization of the nanostructure surface morphology.

ASSOCIATED CONTENT

Supporting Information

Cross-sectional SEM images and EDX spectra of the 1DSiNSAs before and after the removal of AgNPs, details of the simulated device structure and the calculated photogeneration profile (Figures S1−S4) and full sets of optoelectronic parameters used in these simulations (Table S1). This material is available free of charge via the Internet at http://pubs.acs.org.

AUTHOR INFORMATION

Corresponding Author

*E-mail: gacheng@bnu.edu.cn. Telephone and fax: +86-010-62205403.

Notes

The authors declare no competing financial interest.

ACKNOWLEDGMENTS

This work was supported by the National Basic Research Program of China (2010CB832905) and partially funded by the Fundamental Research Funds for the Central Universities and the Program for New Century Excellent Talents in University (NCET).

ABBREVIATIONS

1DSiNSs, one-dimensional Si nanostructures
1DSiNSAs, one-dimensional Si nanostructure arrays
AgNPs, silver nanoparticles
FE-SEM, field emission scanning electron microscope
HR-TEM, high-resolution transmission electron microscope
EDX, energy-dispersive X-ray
μ-PCD, microwave photoconductive decay
FDTD, finite-difference time-domain
SRH, Shockley−Read−Hall
R, photoresponsivity
AA, average absorption
AR, average reflectance
IR, internal photoresponsivity

REFERENCES

(1) Tian, B.; Zheng, X.; Kempa, T. J.; Fang, Y.; Yu, N.; Yu, G.; Huang, J.; Lieber, C. M. *Nature* **2007**, *449*, 885−889.
(2) Zhang, A.; Kim, H.; Cheng, J.; Lo, Y. H. *Nano Lett.* **2010**, *10*, 2117−2120.
(3) Zhang, R. Q.; Liu, X. M.; Wen, Z.; Jiang, Q. *J. Phys. Chem. C* **2011**, *115*, 3425−3428.
(4) Bahruji, H.; Bowker, M.; Davies, P. R. *Int. J. Hydrogen Energy* **2009**, *34*, 8504−8510.
(5) Yan, S.; He, N.; Song, Y.; Zhang, Z.; Qian, J. *J. Electroanal. Chem.* **2009**, *641*, 136−140.
(6) Hochbaum, A. I.; Chen, R.; Delgado1, R. D.; Liang, W.; Garnett1, E. C.; Najarian, M.; Majumdar, A.; Yang, P. *Nature* **2008**, *451*, 163−168.
(7) Peng, P. Q.; Yan, Y. J.; Gao, S. P.; Zhu, J. *Adv. Mater.* **2002**, *14*, 1164−1167.
(8) Zhao, F.; Zhao, D.-d.; Wu, S.-l.; Cheng, G.-a.; Zheng, R.-t. *J. Korean Phys. Soc.* **2009**, *55*, 2681−2684.
(9) Huang, Z.; Geyer, N.; Werner, P.; Boor, J.; Gösele, U. *Adv. Mater.* **2011**, *23*, 285−308.
(10) Peng, K. Q.; Wang, W.; Lee, S. T. *Appl. Phys. Lett.* **2008**, *92*, 163103−163105.
(11) Dalchiele, E. A.; Martín, F.; Leinen, D.; Marotti, R. E.; Ramos-Barrado, J. R. *Thin Solid Films* **2010**, *518*, 1804−1808.
(12) Hagedorn, K.; Forgacs, C.; Collins, S.; Maldonado, S. *J. Phys. Chem. C* **2010**, *114*, 12010−12017.
(13) Wu, S.-l.; Zhang, T.; Zheng, R.-t.; Cheng, G.-a. *Chem. Phys. Lett.* **2012**, *538*, 102−107.
(14) Deinega, A.; John, S. *J. Appl. Phys.* **2012**, *112*, 074327−074333.
(15) Zhu, J.; Yu, Z.; Burkhard, G. F.; Hsu, C.-M.; Connor, S. T.; Xu, Y.; Wang, Q.; McGehee, M.; Fan, S.; Cui, Y. *Nano Lett.* **2009**, *9*, 279−282.
(16) Wen, L.; Zhao, Z.; Li, X.; Shen, Y.; Guo, H.; Wang, Y. *Appl. Phys. Lett.* **2011**, *99*, 143116−143118.
(17) Hu, L.; Chen, G. *Nano Lett.* **2007**, *7*, 3249−3252.
(18) Foley, J. M.; Price, M. J.; Feldblyum, J. I.; Maldonada, S. *Energy Environ. Sci.* **2012**, *5*, 5203−5220.
(19) Wu, S.-l.; Zhang, T.; Zheng, R.-t.; Cheng, G.-a. *Appl. Surf. Sci.* **2012**, *258*, 9792−9799.
(20) Wu, S.-l.; Deng, J.-h.; Zhang, T.; Zheng, R.-t.; Cheng, G.-a. *Diamond Relat. Mater.* **2012**, *26*, 83−88.
(21) Kelzenberg, M. D.; T-Evans, D. B.; Putnam, M. C.; Boettcher, S. W.; Briggs, R. M.; Baek, J. K.; Lewis, N. S.; Atwater, H. A. *Energy Environ. Sci.* **2011**, *4*, 866−871.

(22) Peng, K. Q.; Lu, A. J.; Zhang, R. Q.; Lee, S. T. *Adv. Funct. Mater.* **2008**, *18*, 3026−3035.
(23) Huang, Z.; Geyer, N.; Werner, P.; Boor, J. D.; Gösele, U. *Adv. Mater.* **2011**, *23*, 285−308.
(24) Grätzel, M. *Nature* **2001**, *414*, 338−344.
(25) Adrian, W. B. *Curr. Sep.* **1998**, *17*, 87−91.
(26) Peng, K. Q.; Wang, X.; Wu, X. L.; Lee, S. T. *Nano Lett.* **2009**, *9*, 3704−3709.
(27) Clapham, P. B.; Hutley, M. C. *Nature* **1973**, *244*, 281−282.
(28) Wilson, S. J.; Hutley, M. C. *J. Mod. Opt.* **1982**, *29*, 993−1009.
(29) Branz, H. M.; Yost, V. E.; Scott, W. A. R. D.; Jones, K. M.; To, B.; Stradins, P. *Appl. Phys. Lett.* **2009**, *94*, 231121−231123.
(30) Yablonovitch, E.; Gmitter, T. J. *Solid-State Electron.* **1992**, *35*, 261−267.
(31) Allen, J. E.; Hemesath, E. R.; Perea, D. E.; Lensch-Falk, J. L.; Li, Z. Y.; Yin, F.; Gass, M. H.; Wang, P.; Bleloch, A. L.; Palmer, R. E.; Lauhon, L. J. *Nat. Nanotechnol.* **2008**, *3*, 168−173.
(32) Dan, Y.; Seo, K.; Takei, K.; Meza, J. H.; Javey, A.; Crozier, K. B. *Nano Lett.* **2011**, *11*, 2527−2532.
(33) Koynov, S.; Brandt, M. S.; Stutzmann, M. *Appl. Phys. Lett.* **2006**, *88*, 203107−203109.
(34) Fonash, S. *Solar Cell Device Physics*, 2nd ed.; Academic Press: Burlington, MA, 2010; pp 9−64.
(35) Bao, H.; Ruan, X. *Opt. Lett.* **2010**, *35*, 3378−3340.
(36) Kelzenberg, M. D.; Boettcher, S. W.; Petykiewicz, J. A.; Turner-Evans, D. B.; Putnam, M. C.; Warren, E. L.; Spurgeon, J. M.; Briggs, R. M.; Lewis, N. S.; Atwater, H. A. *Nat. Mater.* **2010**, *9*, 239−245.
(37) Wang, X.; Peng, K. Q.; Pan, X. J.; Chen, X.; Yang, Y.; Li, L.; Meng, X. M.; Zhang, W. J.; Lee, S. T. *Angew. Chem., Int. Ed.* **2011**, *50*, 9861−9865.
(38) Shen, X.; Sun, B.; Yan, F.; Zhao, J.; Zhang, F.; Wang, S.; Zhu, X.; Lee, S. *ACS Nano* **2010**, *4*, 5869−5876.